AGU PUBLICATIONS

JGR

Journal of Geophysical Research: Atmospheres

RESEARCH ARTICLE
10.1002/2015JD024285

Key Points:
- Nonsignificant change of drought in China during 1982–2011 revealed by PDSIARTS model
- PDSIARTS denoted-natural drought dominated interannual changes of agricultural drought survey area
- Thornthwaite and Penman PET-based PDSI overestimated drying trend for whole China including cropland

Correspondence to:
H. Yan,
yanhaon@hotmail.com

Citation:
Yan, H., S.-Q. Wang, J.-B. Wang, H.-Q. Lu, A.-H. Guo, Z.-C. Zhu, R. B. Myneni, and H. H. Shugart (2016), Assessing spatiotemporal variation of drought in China and its impact on agriculture during 1982–2011 by using PDSI indices and agriculture drought survey data, *J. Geophys. Res. Atmos., 121*, 2283–2298, doi:10.1002/2015JD024285.

Received 30 SEP 2015
Accepted 23 FEB 2016
Accepted article online 26 FEB 2016
Published online 14 MAR 2016

Assessing spatiotemporal variation of drought in China and its impact on agriculture during 1982–2011 by using PDSI indices and agriculture drought survey data

Hao Yan[1,2], Shao-Qiang Wang[3], Jun-Bang Wang[3], Hou-Quan Lu[1], An-Hong Guo[1], Zai-Chun Zhu[4], Ranga B. Myneni[5], and Herman H. Shugart[2]

[1]National Meteorological Center, China Meteorological Administration, Beijing, China, [2]Environmental Sciences Department, University of Virginia, Charlottesville, Virginia, USA, [3]Institute of Geographic Sciences and Natural Resources Research, Chinese Academy of Sciences, Beijing, China, [4]Department of Ecology, College of Urban and Environmental Sciences, Peking University, Beijing, China, [5]Department of Earth and Environment, Boston University, Boston, Massachusetts, USA

Abstract Inspired by concerns of the effects of a warming climate, drought variation and its impacts have gained much attention in China. Arguments about China's drought persist and little work has utilized agricultural drought survey area to evaluate the impact of natural drought on agriculture. Based on a newly revised self-calibrating Palmer Drought Severity Index (PDSI) model driven with air-relative-humidity-based two-source (ARTS) E_0 ($PDSI_{ARTS}$; Yan et al., 2014), spatial and temporal variations of drought were analyzed for 1982–2011 in China, which indicates that there was nonsignificant change of drought over this interval but with an extreme drought event happened in 2000–2001. However, using air temperature (T_a)-based Thornthwaite potential evaporation (E_{P_Th}) and Penman-Monteith potential evaporation (E_{P_PM}) to drive the PDSI model, their corresponding $PDSI_{Th}$ and $PDSI_{PM}$ all gave a significant drying trend for 1982–2011. This suggests that PDSI model was sensitive to E_P parameterization in China. Annual drought-covered area from agriculture survey was initially adopted to evaluate impact of PDSI drought on agriculture in China during 1982–2011. The results indicate that $PDSI_{ARTS}$ drought area (defined as $PDSI_{ARTS} < -0.5$) correlated well with the agriculture drought-covered area and $PDSI_{ARTS}$ successfully detected the extreme agriculture drought in 2000–2001 during 1982–2011, i.e., climate factors dominated the interannual changes of agriculture drought area, while $PDSI_{Th}$ and $PDSI_{PM}$ drought areas had no relationship with the agriculture drought-covered area and overestimated the uptrend of agriculture drought This study highlights the importance of coupling PDSI with drought survey data in evaluating the impact of natural drought on agriculture.

1. Introduction

Besides flooding, drought is regarded as the most severe natural hazard. It can persist for several months to several years and thus affects the security of agriculture production, natural ecosystem, and domestic water supply. Drought is often classified into three types [*Mishra and Singh*, 2010]: *Meteorological droughts*, which primarily result from below-normal precipitation over a prolonged period of time; *Hydrological droughts* are characterized by a reduction in stream flow and dropping of the groundwater level; Strong evaporation and diminished precipitation (P_r) cause depletion of soil water and crop wilting to trigger *agricultural droughts*, which threatens food production.

Many drought indices have been developed to monitor drought evolution on seasonal and interannual scales and study its stress impacts on environmental processes and social economic activities [*Mishra and Singh*, 2010; *Mu et al.*, 2013; *Anderson et al.*, 2013]. As a widely used drought index, the Palmer drought severity index (PDSI) [*Palmer*, 1965] uses potential evaporation (E_p) and P_r to drive a two-layer soil water balance model. Standardized precipitation index (SPI) [*McKee et al.*, 1993] solely depends on time series of P_r . Reconnaissance drought index (RDI) [*Tsakiris and Vangelis*, 2005] is calculated from the ratio of P_r to E_P. Recently, standardized precipitation evapotranspiration index (SPEI) [*Vicente-Serrano et al.*, 2012] uses P_r minus E_P to represent the water surplus or deficit.

As a typical hydrological drought index, surface water supply index (SWSI) [*Shafer and Dezman*, 1982] is calculated according to nonexceedance probability from time series of reservoir storage, stream flow, snow pack, and P_r. Because soil water deficiency in the root zone often causes crop damage and loss in crop yield, soil moisture naturally becomes a crop drought index for agricultural drought. Soil moisture is often derived from land surface hydrology models because there is no long-term observation of soil moisture especially on a large spatial scale [*Palmer*, 1965; *Narasimhan and Srinivasan*, 2005; *Wang et al*., 2011].

Development of remote sensing technologies since 1980s has expanded the monitoring methodology for drought. The normalized difference vegetation index (NDVI)-derived Vegetation Condition Index (VCI) [*Kogan*, 1997], the thermal infrared-based evaporative stress index (ESI) [*Anderson et al*., 2011], the passive microwave-retrieved soil moisture [*Owe et al*., 2008], and the terrestrial water storage (TWS) retrieved from the twin-satellite Gravity and Climate Experiment (GRACE) data have been successfully applied to monitoring drought. With an increased remote sensing capability to capture spatial-temporal changes of land surface state on a large scale (e.g., leaf area index (L_{ai}) and soil moisture), remote sensing data and products have been adopted in meteorological, hydrological, and agricultural drought models [*Mu et al*., 2013; *Yan et al*., 2014; *McNally et al*., 2015].

Drought indices provide global drought climatology in response to global warming. Early research indicated a global drying trend during 1950–2008 using Thornthwaite E_{P_Th}-based PDSI [*Dai*, 2011], but recent findings [*Sheffield et al*., 2012] show little change in global drought over the past 60 years (from 1950 to 2008) when evaluated using the Penman–Monteith E_{P_PM}-driven PDSI. This is argued primarily resulting from the PDSI model sensitivity to the driving factor of E_P. Thornthwaite E_{P_Th} shows an increasing trend during past decades attributable to its dependence on temperature and $PDSI_{Th}$ overestimates the increase in global drought [*Sheffield et al*., 2012; *Yan et al*., 2014]. The Penman–Monteith E_{P_PM} incorporates more effects of net radiation, wind speed, and humidity besides temperature, and $PDSI_{PM}$ indicates a result of little change in global drought over the past 60 years [*Sheffield et al*., 2012].

The self-calibrating $PDSI_{ARTS}$ model [*Yan et al*., 2014] replaces E_P with leaf area index-based total evapotranspiration (ARTS E_0) and includes a simple snowmelt module. It shows that global land became wetter mainly due to increased precipitation and the El Niño–Southern Oscillation (ENSO) effect for the period of 1982–2011.

Drought climatology over decades is affected by atmosphere evaporation E_P as well as P_r. Because of the significant correlation between PDSI and observed stream flow as well as soil moisture, PDSI and its revisions have been widely used as standard drought indices for comparison against other drought indices [*Dai*, 2011; *Zhai et al*., 2010; *Vicente-Serrano et al*., 2012].

In middle latitude of Northern hemisphere, China has a large area of arid and semiarid climatic zones where drought affecting regional crop production occurs almost every year. However, there is a considerable argument about the drought trend in the past in China. *Li et al*. [2009] posited a significant decreasing trend in moisture availability and an increasing trend of moisture deficit-affected areas during 1951–2005 across China and Mongolia based on monthly PDSI data. Based on soil moisture simulated with land surface hydrology models driven by a three-hourly meteorological data set over China, *Wang et al*. [2011] also found a drying trend over China for 1950–2006. Similarly, *Yu et al*. [2014a] found that dry area (defined as $SPEI < -1$) has a long-term increasing trend of 3.7% per 10 years ($P < 0.01$) during 1951–2010 based on the SPEI index calculated from monthly P_r and air temperature data at 609 meteorological stations. In contrast, other studies have found neither a long-term upward nor downward trend in drought areas defined as $PDSI < -1$ [*Zou et al*., 2005] or $SPI12 < -0.8$ [*Zhang and Zhou*, 2015]. Based on three drought indices, *Xu et al*. [2014] found no significant trend of drought severity after 1980 and observed that the 1960s featured more serious drought occurrences than other decades.

These different results depend on the choice of drought monitoring model and its parameterization of driving forces. Thus, in this paper we ask, "What kind of drought trend can be deduced when the remote sensing-based $PDSI_{ARTS}$ model [*Yan et al*., 2014] is applied to China?"

A similar and very important issue involves the evaluation of drought impacts on agriculture. Crop yields and drought occurrence statistics are closely related [*Yu et al*., 2014a, 2014b; *Mkhabela et al*., 2010], but consistency analysis of drought trends derived from drought indices and agricultural drought survey is sparse. There is little work relating drought-covered area data derived from agriculture surveys with drought

indices in China [*Zhang and Zhou*, 2015]. China has investigated agricultural drought area for decades, so there is an opportunity to investigate the degree that PDSI drought concurs with agricultural drought surveys on drought area, especially in their climatic trends.

In this paper, we utilize the self-calibrating $PDSI_{ARTS}$ model [*Yan et al.*, 2014] to construct a drought climatology in China over a period of 30 years from 1982 to 2011. This paper is organized as following sections: (1) introduction of $PDSI_{ARTS}$ model; (2) description of remotely sensing vegetation L_{ai} and meteorological data sets, and data processing method; (3) climatology analysis of drought derived from different E_P-driven PDSI models over 1982–2011; (4) consistency analysis of drought areas given by agricultural survey and PDSI indices; and (5) discussion of uncertainties of $PDSI_{ARTS}$ model in agricultural drought evaluation.

2. Methods

2.1. Potential Evaporation Models

As PDSI model is sensitive to driving forcing of potential evaporation (E_P) or reference evaporation (E_0), a novel net radiation-based Penman-Monteith E_P type model (ARTS E_0) [*Yan et al.*, 2014] was applied to driving PDSI model. Conventional temperature-based *Thornthwaite* [1948] and Penman-Monteith [*Monteith*, 1965] E_P models were also adopted for comparison in this study.

2.1.1. ARTS E_0 Module

As a widely cited process approach for modeling E_P, Penman-Monteith E_{P_PM} model [*Monteith*, 1965] is preferred because it accounts for the radiative and aerodynamic processes and for the effects of vegetation physiology. E_{P_PM} typically calculates surface conductance directly from L_{ai} with an assumption of "big leaf" plant canopy and neglecting soil evaporation. By contrast, as a canopy conductance-based two-source model with an assumption of adequate soil water availability, the ARTS E_0 module [*Yan et al.*, 2012] calculates plant transpiration (E_c) and soil evaporation (E_s), respectively,

$$E_0 = E_c + E_s. \tag{1}$$

The net radiation (R_n) is partitioned to a soil part (R_{ns}) [*Impens and Lemeur*, 1969] and a canopy part (R_{nc}),

$$R_{ns} = R_n \exp(-k_A L_{ai}) \tag{2}$$

$$R_{nc} = R_n - R_{ns}, \tag{3}$$

where R_{nc} and R_{ns} are parts of the net radiation that are absorbed by the canopy and the soil, respectively, and k_A equals 0.6 [*Impens and Lemeur*, 1969; *Chen et al.*, 1997].

The canopy transpiration (E_c) model is calculated from a modified Penman-Monteith model with input of the canopy-absorbed net radiation R_{nc} and canopy conductance (G_c),

$$E_c = \frac{\Delta R_{nc} + \rho C_p D G_a}{\Delta + \gamma(1 + G_a/G_c)} \tag{4}$$

$$G_c = g_{smax} \times R_h \times L_{ai}, \tag{5}$$

where R_{nc} is the net radiation absorbed by the canopy; Δ is the gradient of the saturated vapor pressure to air temperature; γ is the psychrometric constant; ρ is the density of air; C_p is the specific heat of air at constant pressure; G_a is the aerodynamic conductance accounting for wind speed impact [*Monteith and Unsworth*, 1990]; G_c is the canopy conductance accounting for transpiration from the vegetation; and D equals $e_s - e_a$ and is the vapor pressure deficit of the air, with e_s is the saturation water vapor pressure at air temperature and e_a is the actual water vapor pressure, R_h is the relative humidity, and g_{smax} is the maximum stomatal conductance assumed to have a value of 12.2 mm s^{-1} [*Kelliher et al.*, 1995]. L_{ai} is the leaf area index used for scaling stomatal conductance to canopy conductance for a large-scale application of the Penman-Monteith equation.

The soil evaporation (E_s) equation is modified from an air relative-humidity-based evapotranspiration model (ARM-ET) [*Yan and Shugart*, 2010],

$$E_s = 1.35 R_h \frac{\Delta R_{ns}}{\Delta + \gamma} \tag{6}$$

which scales the *Priestley and Taylor* [1972] equilibrium evaporation to wet surface E_s by using R_h as a complementary relationship coefficient with an assumption of adequate soil water availability. However, in soil

water stressed region, soil water balance model is still required to calculate actual soil evaporation from E_s [*Yan et al.*, 2012].

2.1.2. Thornthwaite E_{P_Th} Module

The original *Palmer* [1965] PDSI model adopts the simple *Thornthwaite* [1948] E_P equation, which depends only on variables of monthly mean air temperature, latitude, and month. A modified Thornthwaite E_P equation (E_{P_Th}) [*Karl*, 1986] is applied in this study,

$$E_{P_{Th}} = \begin{cases} 0 & \text{if } T_a \le 0^oC \\ 25.4 d_u \exp[-3.8633 + 1.7156B - B\ln(H) - B_u \ln(T_a)] & \text{if } 0 < T_a < 26.7^oC \\ 25.4 d_u \left[\sin(T_a/57.3 - 0.166) - 0.76\right] & \text{if } T_a \ge 26.7^oC \end{cases} \quad (7)$$

$$H = \sum_{m=1}^{12} \left(\frac{\max(T_a, 0)}{5}\right)^{1.514} \quad (8)$$

$$B = 0.492 + 1.79\times10^{-2}H - 7.71\times10^{-5}H^2 + 6.75\times10^{-7}H^3 \quad (9)$$

$$d_u = \begin{cases} (d_0 + 0.0157)/1.57 & \text{if } d_0 \ge 0 \\ (3.141593 + d_0 + 0.0157)/1.57 & \text{if } d_0 < 0 \end{cases} \quad (10)$$

$$d_0 = \tan^{-1}\left(\sqrt{\frac{\max\left(0.1, 1 - [\varphi(m)\tan(\theta)]^2\right)}{-\varphi(m)\tan(\theta)}}\right), \quad (11)$$

where T_a is monthly average air temperature (°C) at 2 m height, $\varphi(m)$ is a month (m)-dependent coefficient, θ is the latitude, and B and H are two heat factors.

2.1.3. Penman-Monteith E_{P_PM} Module

Penman-Monteith E_{P_PM} [*Monteith*, 1965], which combines the radiative and aerodynamic processes, has been adopted in recent PDSI drought researches [*Sheffield et al.*, 2012; *van der Schrier et al.*, 2011].

$$E_{p\_pm} = \frac{\Delta R_n + 6.43(1 + 0.536u)D}{\Delta + \gamma}, \quad \text{(B6)}$$

where E_{P_PM} is potential evapotranspiration (mm d^{-1}), R_n is net radiation, Δ is the gradient of the saturated vapor pressure to the air temperature (kPa), γ is the psychrometric constant, D is the vapor pressure deficit, and u is the wind speed (m s^{-1}) at 2 m height.

2.2. A Snow-Melting and Accumulation Module

With a temperature threshold of 0°C, precipitation P_r is divided into precipitation and snowfall; snowfall is then added to the snowpack (S_{now}). Snowmelt is calculated from snowpack using a temperature-based snowmelt function [*Yan et al.*, 2012]. The water supply P, defined as the sum of precipitation and snowmelt, is used to substitute for P_r to drive the self-calibrating PDSI model on a monthly scale in this study,

$$P = P_r + S_{now} \times S_f \quad (12)$$

$$S_f = \begin{cases} 0 & \text{if } T_a \le 0^oC \\ 0.2T_a & \text{if } 0^oC < T_a \le 5^oC \\ 1 & \text{if } T_a > 5^oC \end{cases}. \quad (13)$$

where P is the water input (mm $month^{-1}$) including precipitation (P_r) and snowmelt, S_f is the snow-melting factor, and T_a is the air temperature (°C).

2.3. Self-Calibrating ARTS PDSI Model

The original *Palmer* PDSI model [1965] was developed in the U.S. Great Plains. Its weighting and duration factors, derived from local calibration against a limited amount of observed data, prompted *Wells et al.* [2004] to point out a lack of consistency when making comparisons between different climatological regions. To solve this shortcoming, a self-calibrating PDSI model has been developed [*Wells et al.*, 2004] and considered prior in global drought monitoring [*Dai*, 2011; *Van der Schrier et al.*, 2011; *Yan et al.*, 2014].

The $PDSI_{ARTS}$ model [*Yan et al.*, 2014] further couples the self-calibrating PDSI model [*Wells et al.*, 2004] with the ARTS E_0 module and snow-melting module (see sections 2.1 and 2.2) to account for the effects of calibration coefficients, seasonal vegetation, and snow melting. The water supply P, defined as the sum of precipitation and snowmelt derived from the simple snow-melting module (see section 2.2), drives self-calibrating PDSI

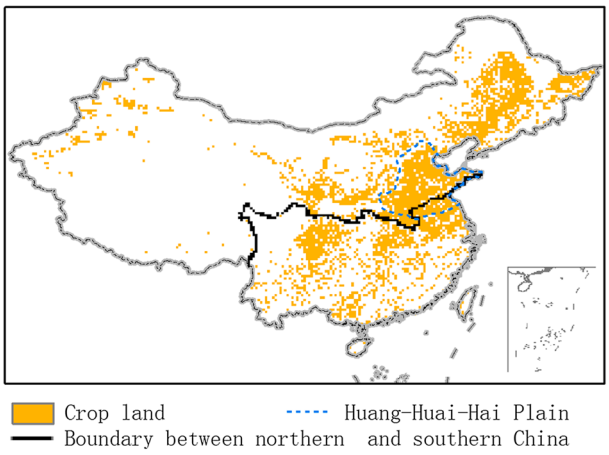

Figure 1. Distribution of crop land in China, Huang-Huai-Hai (HHH) Plain, and the boundary showing northern and southern China.

model instead of the more usual P_r. The $PDSI_{ARTS}$ model has been applied to global drought study and its detailed description can be found in *Yan et al.* [2014].

3. Data Sets and Preprocessing

China has a variety of climate zones (i.e., tropical zone, subtropical zone, warm-temperate zone, cold-temperate zone, and plateau zone) distributed from south to north, respectively. Annual precipitation also has a large spatial variability across China with decreases from south to north and from east to west. There are large areas of desert in northwestern China with sparse vegetation and precipitation often less than 100 mm yr^{-1}. Note that Taiwan region is not included in this study due to lack of available forcing data. Agricultural land use data (Figure 1) is adopted from the Chinese national land cover database (ChinaCover2010) produced by the Institute of Remote Sensing and Digital Earth, Chinese Academy of Sciences [*Zhang et al.*, 2014].

3.1. Climate Data

Meteorological data from 756 stations in China were collected from National Meteorological Information Center (NMIC; http://cdc.nmic.cn/home.do) of Chinese Meteorological Administration (CMA). After strict quality control, 571 stations were chosen in this study with continuous length of data covering the period of 1982–2011. Monthly observations including precipitation, air temperature, wind speed, actual water vapor pressure, and relative humidity were then interpolated at a spatial resolution of 0.25° × 0.25° latitude/longitude using a thin plate spline interpolation method.

Daily observations (i.e., sunshine duration, air temperature, and actual water vapor pressure) were also interpolated for calculating daily net radiation (R_n) according to Food and Agriculture Organization (FAO) method [*Allen*, 1998],

$$R_n = (1-\alpha)R_s - R_{nl} \tag{14}$$

$$R_s = \left(0.25 + 0.5\frac{n}{N}\right)R_a \tag{15}$$

$$R_{nl} = \sigma(T_a + 273.15)^4(0.39 - 0.058\sqrt{e_a})\left(0.9\frac{n}{N} + 0.1\right), \tag{16}$$

where R_n is the net radiation (MJ m^{-2} d^{-1}), α is the albedo, R_s is the solar radiation (MJ m^{-2} d^{-1}), R_{nl} is the net longwave radiation (MJ m^{-2} d^{-1}), n is the actual sunshine duration (h), N is the maximum possible sunshine duration (h), R_a is the extraterrestrial radiation (MJ m^{-2} d^{-1}), σ is the Stefan-Boltzmann constant (4.903×10^{-9} MJ K^{-4} m^{-2} d^{-1}), T_a is the air temperature (°C), and e_a is the actual water vapor pressure (kPa). α, featuring seasonal variations, was obtained from 5 year average monthly albedo data derived from advanced very high resolution radiometer (AVHRR) data [*Csiszar*, 2009]. R_s, N, R_a, and R_{nl} were calculated from solar constant, latitude, elevation, and the number of the day in the year. To calculate monthly ARTS E_0, daily R_n was further summed to monthly R_n.

As R_n represents radiation contribution to E_P and ARTS E_0 that affect the variation of PDSI, reliable R_n is desired. Estimated R_n was evaluated against observed R_n at a flux tower in Qianyanzhou station [*S. Wang et al.*, 2015] of southern China for 3 years. Figure 2 shows that estimated R_n successfully captured seasonal variations of R_n with a monthly statistics of $R^2 = 0.97$, Bias = 15.0 W m^{-2}, and Rmse = 19.2 W m^{-2}, which indicates that the FAO method [*Allen*, 1998] can be applied to calculating R_n for drought research of China.

3.2. Global Inventory Modeling and Mapping Studies (GIMMS) Leaf Area Index Data

The latest global leaf area index data set (LAI3g), for the period from July 1981 to December 2011, was generated at 15 day temporal intervals and 8 km spatial resolutions from GIMMS AVHRR normalized

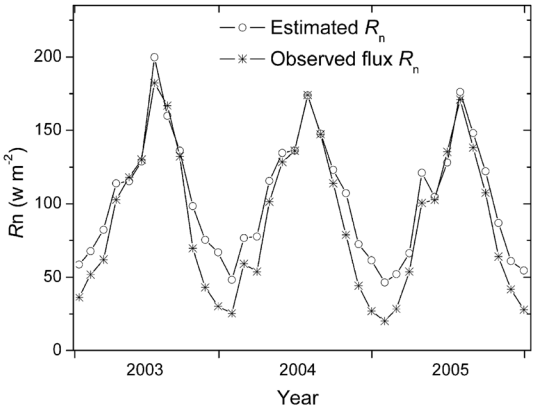

Figure 2. Time series of estimated and observed monthly R_n at Qianyanzhou station during 2003–2005.

difference vegetation index (NDVI) third generation (3 g) data set using an artificial neural network (ANN) model [*Zhu et al.*, 2013]. The ANN model was trained with best quality collection 5 Moderate Resolution Imaging Spectroradiometer (MODIS) L_{ai} product and overlapping GIMMS NDVI3g data for the period of 2000–2009 and then applied to generating LAI3g data set from GIMMS NDVI3g data for prior period of 1982–1999. The 30 year remote sensing L_{ai} data set initially reveals a climate-related change in vegetation, which has been successfully used in research of global land evapotranspiration [*Yan et al.*, 2013], global PDSI drought monitoring and the impact of ENSO [*Yan et al.*, 2014], the weakening relationship between interannual temperature variability and northern vegetation activity [*Piao et al.*, 2014], and the contribution of semiarid ecosystems to interannual variability of global carbon cycle [*Poulter et al.*, 2014].

3.3. Gridded Soil Database

The available water capacity (M_{awc}) for the whole soil profile as required in the ARTS PDSI model was adopted from the "Global Gridded Surfaces of Selected Soil Characteristics" data set developed by *Global Soil Data Task Group* [2000] of the International Geosphere-Biosphere Programme (IGBP)-Data and Information System (DIS). The data set contains seven parameters (soil-carbon density, total nitrogen density, field capacity, wilting point, profile available water capacity, thermal capacity, and bulk density) at a resolution of 5×5 arc minutes.

3.4. Drought-Covered Area Data From Agricultural Survey in China

The drought-covered area data have been investigated by National Bureau of Statistics of China since 1950 with breaks in 1967–1969. The indicator of drought-covered area is defined as planted area of crops in which drought causes more than 10% loss of expected crop yields in a normal year. The survey data provide ground-based observations for evaluating drought indices and for relating hydrometeorological drought with agriculture drought. Note that drought-covered area is referred as drought-affected area by some researchers [*Zhang and Zhou*, 2015].

3.5. Data Processing

All model forcing data including GIMMS L_{ai}, meteorological data, and maximum soil available water content data were interpolated to a $0.25° \times 0.25°$ grid resolution. L_{ai} and station-observed meteorological data (i.e., precipitation, air temperature, relative humidity, wind speed, and net radiation) were then applied to calculating ARTS E_0 and driving $PDSI_{ARTS}$ model on a monthly scale. The $PDSI_{ARTS}$ model used the entire data period of 1982–2011 as calibration interval. To compare the impact of self-calibrating PDSI model driving with different parameterization of E_P on drought trend, we calculated the $PDSI_{ARTS}$ model driven with the E_{P_Th} [*Thornthwaite*, 1948] and E_{P_PM} [*Monteith*, 1965] instead of ARTS E_0. The resultant time series of ARTS E_0, E_{P_Th}, E_{P_PM}, and their corresponding PDSI values were then analyzed and compared with drought-covered area of agricultural survey

Table 1. Classification of Dry and Wet Degree as Defined by Palmer PDSI Index

PDSI	Class	PDSI	Class
4.0 ≤ PDSI	Extremely wet	−1.0 to -0.5	Incipient drought
3.0 to 4.0	Very wet	−2.0 to -1.0	Mild drought
2.0 to 3.0	Moderately wet	−3.0 to -2.0	Moderate drought
1.0 to 2.0	Slightly wet	−4.0 to -3.0	Severe drought
0.5 to 1.0	Incipient wet spell	PDSI ≤ -4.0	Extreme drought
-0.5 to 0.5	Near normal		

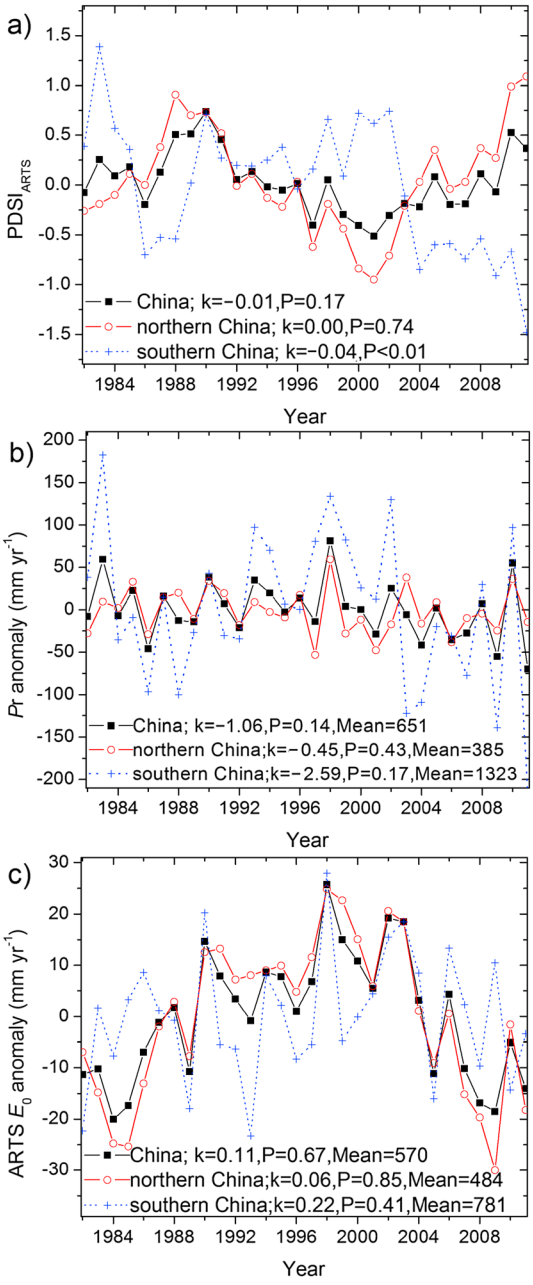

Figure 3. Time series of annual (a) average PDSI$_{ARTS}$, (b) P_r anomaly, and (c) ARTS E_0 anomaly in whole China, northern China, and southern China during 1982–2011, and slope k and significance P of their linear regression as well as climate mean values.

for the same period of 1982 to 2011. The Pearson correlation coefficient R and significance level P were used to analyze changes of drought trend on interannual scale (Table 1).

4. Results

4.1. Drought Trend of PDSI$_{ARTS}$ in China From 1982 to 2011

Time series of annual average PDSI$_{ARTS}$ (Figure 3 a), averaged from monthly PDSI$_{ARTS}$ for whole China, showed no significant change ($P = 0.17$, Table 2) of drought during 1982–2011. Similarly, *Xu et al.* [2014] found that drought severity shows a nonsignificant increasing trend from 1980 to 2012, based on three drought indices of SPI3 (3 months standardized precipitation index), RDI3 (3 months reconnaissance drought index), and SPEI3 (3 months standardized precipitation evapotranspiration index). However, there was a drying trend ($P < 0.01$) during 1990–2000 with year 1990 representing the wettest year and year 2000 featuring a drier climate (Figure 3a). After 2000, a wetting trend ($P < 0.01$) was obtained with year 2011 showing a wetter climate and there was a turning period in 2000 and 2001. This was contrary to previous research that severe and extreme droughts had been more serious in the period of late 1990s to 2010 for all of China based on SPEI data [*Yu et al.*, 2014a].

The nonsignificant change of PDSI$_{ARTS}$ drought in China can be attributed to its two driving forces, i.e., P_r (Figure 3b) and ARTS E_0 (Figure 3 c), which also showed no significant change during 1982–2011. This agrees with the statistically nonsignificant drying trend in the midlatitudes (23°N–48°N) of the Northern Hemisphere due to weak variation of ARTS E_0 and P_r, but it contrasted with the global wetting trend due to increased precipitation and El Niño–Southern Oscillation (ENSO) effect for the same period [*Yan et al.*, 2014]. However, the wetting trend of PDSI$_{ARTS}$ during 2000–2011 (Figure 3a) primarily resulted from a decreasing trend of ARTS E_0 ($P < 0.01$, see Figure 3c and Table 2).

Drought condition denoted by PDSI$_{ARTS}$ was determined not only by annual values of E_0 and P_r for China but also by spatial pattern of E_0 and P_r in northern China and southern China. Comparatively, northern China is about 2.5 times bigger in area than southern China (Figure 1) and featured a rather dry climate with average $P_r = 385$ mm yr^{-1} (Figure 3b) and $E_0 = 484$ mm yr^{-1} (Figure 3c), while southern China had a wet climate with average $P_r = 1323$ mm yr^{-1} and $E_0 = 781$ mm yr^{-1}. Thus, drought events often occurred in northern China compared with southern China. Year 1990 had a positive P_r anomaly in both northern China and southern China (Figure 3b) resulting in a wetting condition for China (Figure 3a), while year 2001 had a higher negative P_r anomaly in northern China and a positive E_0 anomaly plus accumulated effect of previous drought in 2000

Table 2. Trends of $PDSI_{ARTS}$ and Its Driving Forces of P_r ($mm\,yr^{-1}$) and ARTS E_0 ($mm\,yr^{-1}$) During Three Periods of 1982–2011, 1990–2000, and 2000–2011, Respectively

Period	$PDSI_{ARTS}$	P_r	ARTS E_0
1982–2011	$R=-0.25$ ($P=0.17$)	$R=-0.27$ ($P=0.14$)	$R=0.08$ ($P=0.66$)
1990–2000	$R=-0.85$ ($P<0.01$)	$R=0.00$ ($P=0.99$)	$R=0.31$ ($P=0.35$)
2000–2011	$R=0.86$ ($P<0.01$)	$R=-0.18$ ($P=0.57$)	$R=-0.78$ ($P<0.01$)

for northern China (Figure 3), which resulted in the driest condition in 2001 for China (Figure 3a). In other words, annual value of E_0 and P_r for China might not accurately reflect dry or wet condition of whole China because their spatial patterns were also important, i.e., northern China dominated the drought variations of whole China, while southern China played a minor role (Figure 3a).

$PDSI_{ARTS}$ had a complicated spatial distribution of drought trend during 1982–2011 (Figure 4a). Drying trends can be found in southern China and Northeast China, which can be attributed to a deceasing water supply of P_r with a trend of $-1\sim-6\,mm\,yr^{-1}$ (Figure 4b) and an increasing evaporation demand with a trend of $1\sim4\,mm\,yr^{-1}$shown by ARTS E_0 (Figure 4c). A wetting trend dominated western China (Figure 3a) mainly due to an increasing water supply of P_r (Figure 4b). Similarly, *Zhang and Zhou* [2015] pointed out a drying trend in Northeast China and a wetting trend in Northwest China for 1950–2010.

The Huang-Huai-Hai (HHH) Plain has a large crop area planted with spring wheat and summer maize. It is regarded as a major crop planting region in northern China (Figure 1), and it is often subject to drought [*Q. Wang et al.*, 2015]. However, Figure 4a shows a wetting trend in the HHH Plain during 1982–2011, which is consistent with the alleviating trend of drought [*Q. Wang et al.*, 2015] in the HHH plain derived from daily SPEI data sets calculated from daily sunshine duration, P_r, air temperature data for the period of 1981–2010. The drought situation in the HHH Plain does not worsen under warming during the research period. The wetting trend was mainly due to more P_r (Figure 4b) and decreasing evaporation of ARTS E_0 (Figure 4c).

4.2. Spatial Variations of $PDSI_{ARTS}$ Drought for Periods of 1990s and 2000s

Figures 5a and 5b show an opposite spatial distribution of drought trend for periods of 1990–2000 and 2000–2011, respectively. There was a drying trend of $PDSI_{ARTS}$ during 1990–2000 (Figure 5a) followed by a wetting trend for 2000–2011 (Figure 5b) in northern China. Conversely, southern China demonstrated a wetting trend during 1990–2000 (Figure 5a) with a drought trend developing during 2000–2011 (Figure 5 b). The variation of drought during 1990–2000 can be summarized as "southern wet and northern drought" (Figure 5a) and the period of 2000–2011 featured a different spatial pattern of drought, i.e., "Southern drought and Northern wet."

Similarly, there was less water supply of P_r with a trend of $-5\sim-20\,mm\,yr^{-1}$ during the drying period of 1990–2000 (Figure 5c) and then more P_r with an uptrend of $5\sim20\,mm\,yr^{-1}$ during the wetting period of 2000–2011 (Figure 5d) in northern China, and vice versa in southern China. ARTS E_0 had an uptrend ($2\sim10\,mm\,yr^{-1}$) in Northeast China and West China during the drying period of 1990–2000 (Figure 5e) but a downtrend ($-2\sim-10\,mm\,yr^{-1}$) in northern China during the wetting period of 2000–2011 (Figure 5f). Overall, water supply P_r combined with evaporation demand of E_0 determined drought trends in southern China and northern China (Figures 5a and 5b).

Figure 6 shows typical characteristics of northern drought and southern wet under a typical dry climate of 2000 and 2001. Annual average $PDSI_{ARTS}$ (Figure 6a) indicated that drought (defined as $PDSI_{ARTS}<-1$) affected most northern China while a wet climate (defined as $PDSI_{ARTS}>1$) featured most southern China. This coincided with the spatial distribution of P_r (Figure 6b) that there were less P_r ($-5\%\sim-30\%$) in most northern China but more P_r ($5\%\sim15\%$) in most southern China. In addition, ARTS E_0 indicated a higher evaporation demand by $1\%\sim15\%$ relative to climate value averaged over 30 years in most northern China (Figure 6c).

4.3. Comparison of $PDSI_{ARTS}$ With $PDSI_{Th}$ and $PDSI_{PM}$ in China

Time series of annual average $PDSI_{Th}$ and $PDSI_{PM}$ (Figure 7a) indicated a drying trend ($P<0.05$) for whole China during 1982–2011, because its driving forcing of E_{P_Th} and E_{P_PM} (Figure 7b) had an increasing trend

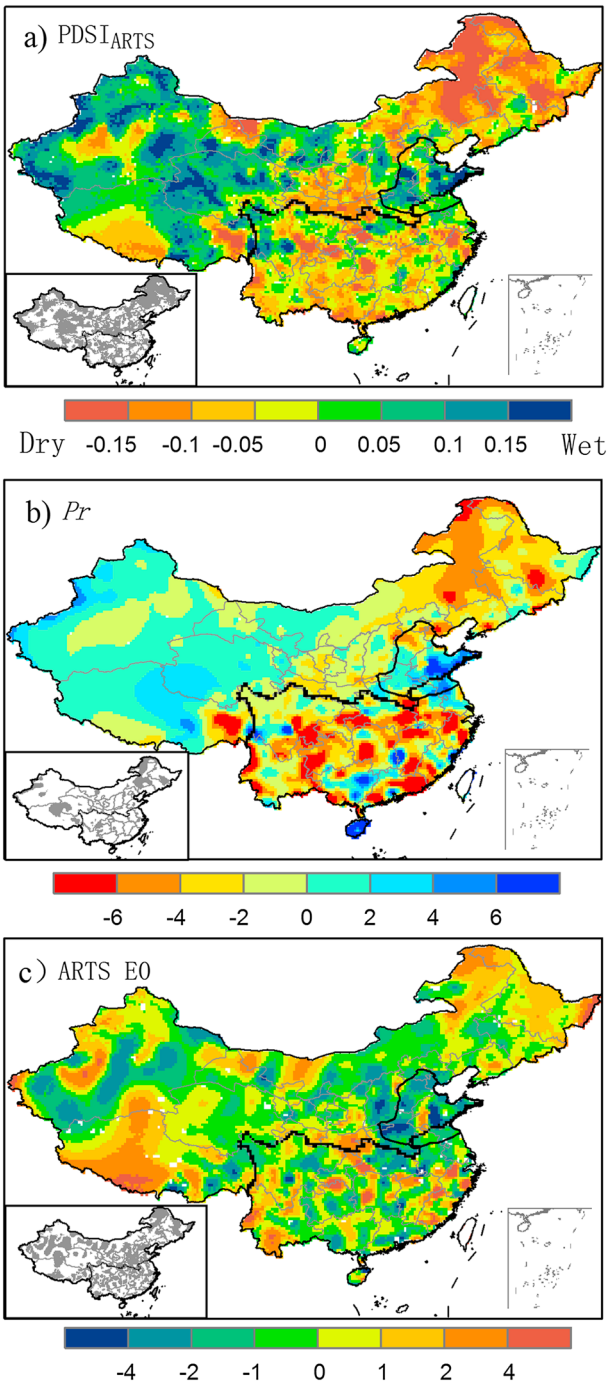

Figure 4. Linear trends of annual (a) average PDSI$_{ARTS}$, (b) P_r (mm yr^{-1}), and (c) ARTS E_0 (mm yr^{-1}), and their significance ($P < 0.05$ shown in gray color in the hatch) of linear trend for period of 1982–2011, respectively.

($P < 0.01$), which was contrary to the non-significant drought trend derived from PDSI$_{ARTS}$ for the same period (Figure 3a).

Figure 8 shows spatial trends of annual average PDSI$_{Th}$ and PDSI$_{PM}$ and corresponding E_{P_Th} and E_{P_PM} during 1982–2011, respectively. Most China featured a drying trend given by PDSI$_{Th}$ (Figure 8a) primarily due to an increasing trend (1 ~ 5 mm yr^{-1}) of E_{P_Th} (Figure 8c). PDSI$_{PM}$ had a similar drought pattern to PDSI$_{Th}$ over most China (Figure 8b) except in western China and Huang-Huai-Hai (HHH) Plain due to a decreasing trend of E_{P_PM} (Figure 8d).

Further analysis of evaporation factors indicates an uptrend of air temperature with an increase of 0.5°C per 10 years (Figure 9a) for whole China during 1982–2011, which contributed to the significant increasing trend ($P < 0.01$) of E_{P_Th} and hence the drying trend of PDSI$_{Th}$ (Figures 7a and 7b) for the same period. Spatial distribution of annual average T_a also showed an increasing trend of 0.1 ~ 1.5°C per 10 years in most China, especially western China (Figure 9a). In contrast, surface incident solar radiation Q (Figure 9b) had no significant trend ($P = 0.43$) during 1982–2011 and regions having increasing or decreasing trend of Q geographically dispersed over China. According to the Penman-Monteith [*Monteith*, 1965] evaporation theory, both T_a and Q are important energy factors and thus should be taken into consideration in calculating the potential evaporation, especially due to their different spatial-temporal variations in China. In addition, W_s, as a factor of aerodynamic process in E_{P_PM}, significantly decreased during the research period (Figure 9c). As a result, E_{P_PM} had a lower uptrend than that of E_{P_Th}, and PDSI$_{PM}$ showed a drying trend but less serious than that of PDSI$_{Th}$ (Figure 7a). As a key variable in calculating plant transpiration and soil evaporation of ARTS E_0, R_h had a decreasing trend ($P < 0.01$) of 0.7% per 10 years in China (Figure 9d), especially after 2003, which contributed to the decreasing evaporation demand of ARTS E_0 besides W_s.

4.4. Agricultural Droughts in China From 1982 to 2011

Many croplands are planted with one-season crop in Northeast China and western China, but there are extensive areas with two-season crops such as winter wheat and summer maize in the Huang-Huai-Hai (HHH) Plain

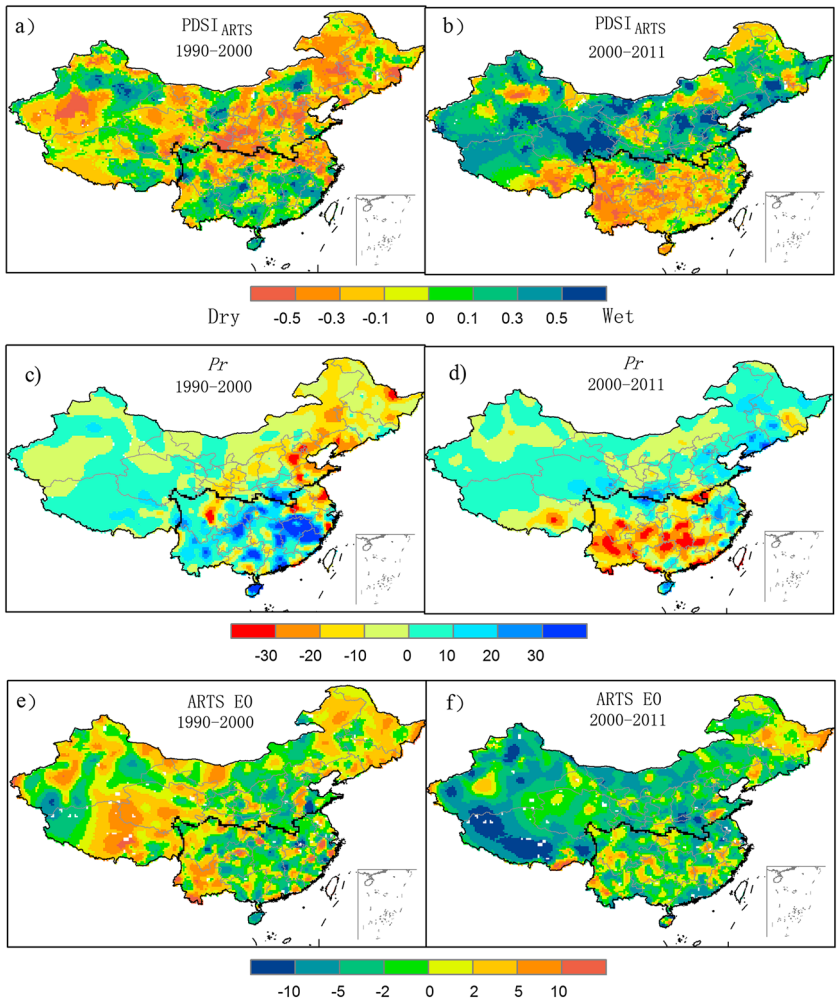

Figure 5. Linear trends of annual (a, b) average $PDSI_{ARTS}$, (c, d) P_r (mm yr^{-1}), and (e, f) ARTS E_0 (mm yr^{-1}) during (left) 1990–2000 and (right) 2000–2011.

and Southwest China. In these latter cases, the drought-covered area is likely to be counted twice on a particular field by agriculture survey. Similarly, PDSI drought area, defined as average PDSI < -0.5, was calculated for crop growing period with regard to one-season crops. For two-season crops, PDSI drought area was calculated twice on a particular field according to corresponding crop growing period so that PDSI and survey drought areas could be compared. Figure 10a shows that $PDSI_{ARTS}$ drought area over crop land correlated well ($P < 0.01$) with the survey area, i.e., $PDSI_{ARTS}$ had a potential to indicate the interannual changes of agricultural drought area in China.

$PDSI_{ARTS}$ drought area for crop land had an increasing trend ($P < 0.05$, $k = 1.2 \times 10^4$ km^2 yr^{-1}) from 1982 to 2011 (Figure 10a). However, drought survey area had no significant change ($P = 0.51$) from 1982 to 2011. Both drought areas over cropland reached a maximum in 2000 and 2001 and then declined until 2005 (Figure 10a). It means that both year of 2000 and 2001 representing a typical drought event resulted in the extreme disaster of agriculture drought during the research period.

Figure 10b shows that $PDSI_{Th}$ and $PDSI_{PM}$ drought area over cropland significantly increased ($P < 0.01$) by 3.5×10^4 and 2.2×10^4 km^2 yr^{-2} during 1982–2011, respectively, and they had no relationship ($P > 0.2$) with the drought-covered area from agriculture survey. In other words, $PDSI_{Th}$ and $PDSI_{PM}$ were unable to detect the interannual changes of agriculture drought area in China. Besides, the abrupt increase of agricultural drought area given by $PDSI_{Th}$ and $PDSI_{PM}$ was contrary to the nonsignificant change of drought area from agriculture survey.

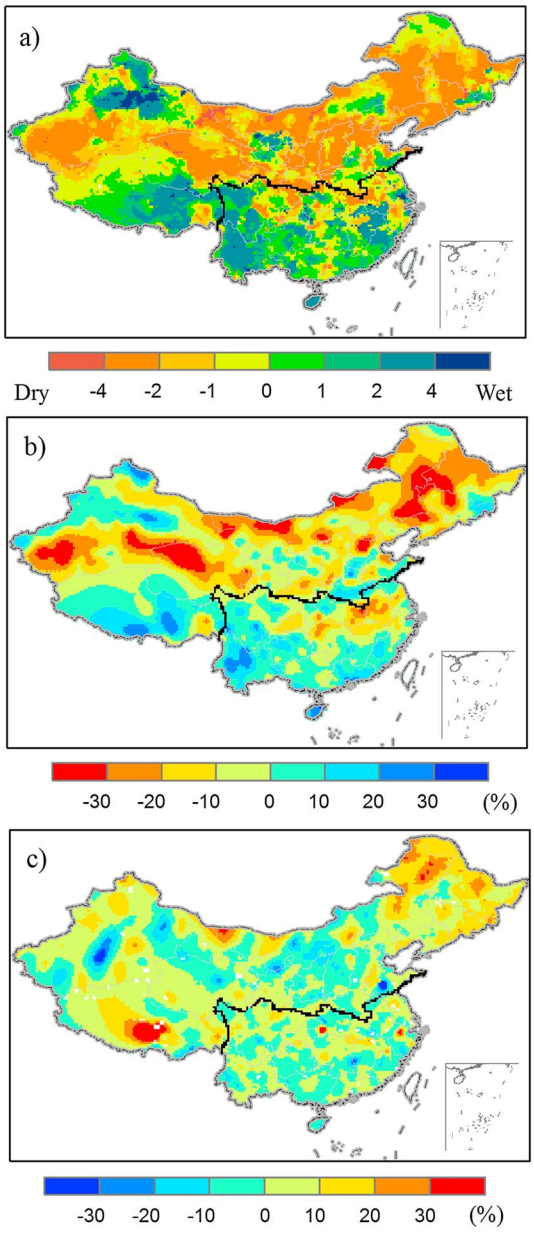

Figure 6. Spatial pattern of (a) average $PDSI_{ARTS}$, anomaly percentage of (b) P_r and (c) ARTS E_0 for 2000 and 2001.

5. Discussion

PDSI model mainly reveals natural drought variations and its evolution is strongly affected by variations of precipitation belt in monsoon regions, especially in China. Because China features the East Asia monsoon climate dominated by the anticyclone circulation over western Pacific (the western Pacific subtropical high) that controls shifting of precipitation belt [*Zhou and Yu*, 2005], its abnormal movements and intensity changes often produce droughts as well as floods. Past changes of the East Asia monsoon is likely related to ENSO activities and variations in land-ocean thermal contrasts [*Lau et al.*, 2000; *Li et al.*, 2007], and an exceptional drought event in 1965–1966 over eastern China results from a significant reduction of summer monsoon precipitation amplified by volcanic eruption and an El Niño event [*Shen et al.*, 2007]. This was also found in this study that the $PDSI_{ARTS}$ drying trend in northern China from 1990 to 2000 (Figure 5a) could be mainly attributed to the decreasing P_r (Figure 5c), which can be summarized as "southern wet and northern drought" indicating a close relationship with shifting of monsoon precipitation belt. In addition, recent climate models [*Sun and Ding*, 2010] project an enhanced precipitation in the future over most of China due to increases in both monsoon circulation and water vapor transport in response to the global warming, which might make up for the drying trend resulted from warming-related enhancement of atmosphere evaporation [*Sheffield and Wood*, 2008]. It can be concluded that regional warming does not necessarily produce regional drying, and drought status in the future depends on many other factors such as precipitation, surface solar radiation, air humidity, and wind speed. However, global warming is likely causing drought to set in more quickly and with greater intensity [*Trenberth et al.*, 2014].

In concept, the PDSI derived-drought area over crop land is different from the drought-covered area from agriculture survey, especially in China, because the drought survey data reflect combined results of climate factors, irrigation, and agricultural practices, and other human influences. There are some factors related with agriculture drought but not considered in current PDSI models. For instance, agricultural drought is potentially affected by atmosphere CO_2 concentrations. During past century as well as the research period of 1982–2011, atmospheric CO_2 increase and global warming have characterized climatic change [*Hartmann et al.*, 2013]. Many experiments and studies have found that elevated-CO_2 increases water use efficiency (WUE) by sustaining photosynthesis of water-limited crops at a lower stomatal conductance [*Tuba et al.*, 1994; *Brodribb et al.*, 2009; *Allen et al.*, 2011; *Li et al.*, 2013], which implies an adaptation to drought stress for stressed plants at elevated CO_2 by delaying the adverse effects of drought and maintaining photosynthesis for extra days [*Vu and Allen*, 2009]. *Allen et al.* [2011] further found that drought-induced loss of biomass for plants is lower at elevated CO_2 than that at

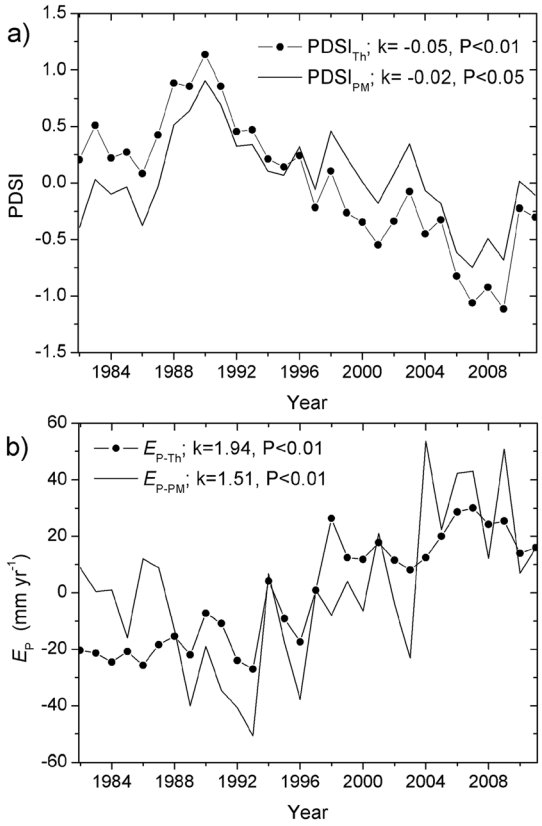

Figure 7. Time series of annual (a) average $PDSI_{Th}$ and $PDSI_{PM}$ and (b) E_{P_Th} and E_{P_PM} for whole China during 1982–2011.

ambient CO_2, i.e., elevated CO_2 can alleviate the impact of drought on crop yield. However, the impact of CO_2 has not been considered in current PDSI models.

In addition, the technology of cultivation and breeding in crops and the building of irrigation facility contribute to an enhanced drought resistant capacity in agriculture of China [*Wu et al.*, 2010]. As a result, light drought such as incipient drought defined by $-1.0 < PDSI_{ARTS} < -0.5$ might have a decreasing impact on crop yield and corresponding agricultural drought area would gradually decline. This might help explain the nonsignificant change of agriculture survey area of drought in China during 1982–2011 (Figure 10a). Biological, agrotechnical, and atmosphere CO_2 impacts make agricultural drought different from PDSI drought and more challenging to be quantitatively monitored by using current drought indices, especially from a perspective of climatic change. It is our assessment that these factors, e.g., atmospheric CO_2 increase and cultivation technology, alleviated the impacts of nature drought derived from PDSI on agriculture in China. Yet, these impacts, neglected by current PDSI models, need further mechanism-based research and are clearly the challenge for future drought model studies.

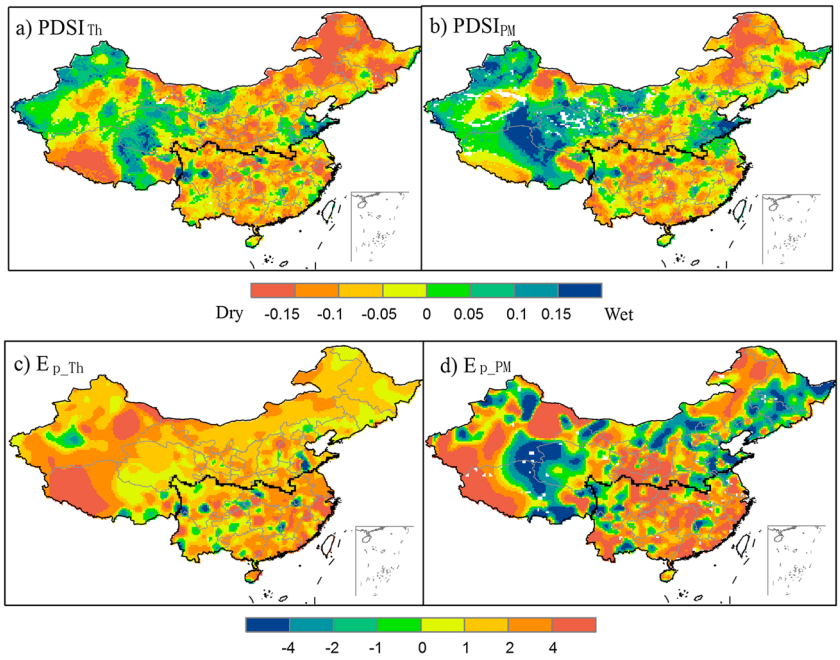

Figure 8. Linear trends of annual average (a) $PDSI_{Th}$, (b) $PDSI_{PM}$, (c) E_{P_Th} (mm yr^{-1}), and (d) E_{P_PM} (mm yr^{-1}) for period of 1982–2011, respectively.

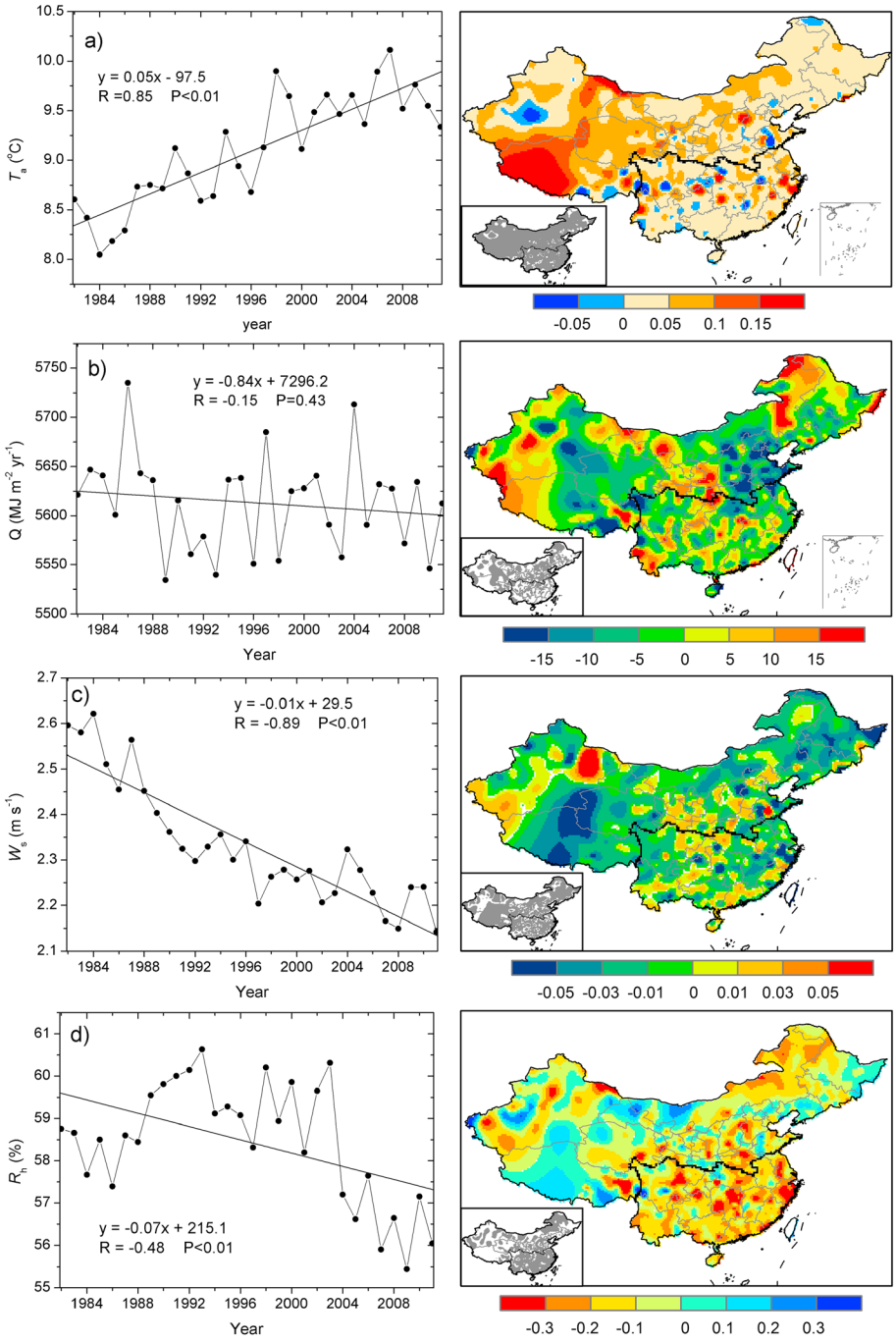

Figure 9. (left) Time series of annual (a) average T_a, (b) surface solar radiation Q, (c) average W_s, and (d) average R_h and (right) their linear trends and significance ($P < 0.05$ shown in gray color in the hatch) in China during 1982–2011.

From the view of physical parameters and PDSI model complexity, the key driving force of potential evaporation E_P should be explored because PDSI is sensitive to E_P [*Sheffield et al.*, 2012; *Yan et al.*, 2014]. E_{P_Th} includes only one parameter of temperature and E_{P_PM} considers temperature, radiation, wind speed, and vapor pressure deficit. ARTS E_0 as a two source E_P model considers contributions of vegetation transpiration and soil evaporation by including two more parameters of LAI and relative humidity than E_{P_PM} [*Yan et al.*, 2014]. As remote sensing LAI is capable of reflecting drought condition of vegetation, ARTS E_0-driven $PDSI_{ARTS}$ indirectly considered the impact of drought on vegetation including crops, which is a major feature of $PDSI_{ARTS}$. In contrast, $PDSI_{PM}$ and $PDSI_{Th}$ do not consider the impact of real vegetation in drought monitoring. In theory,

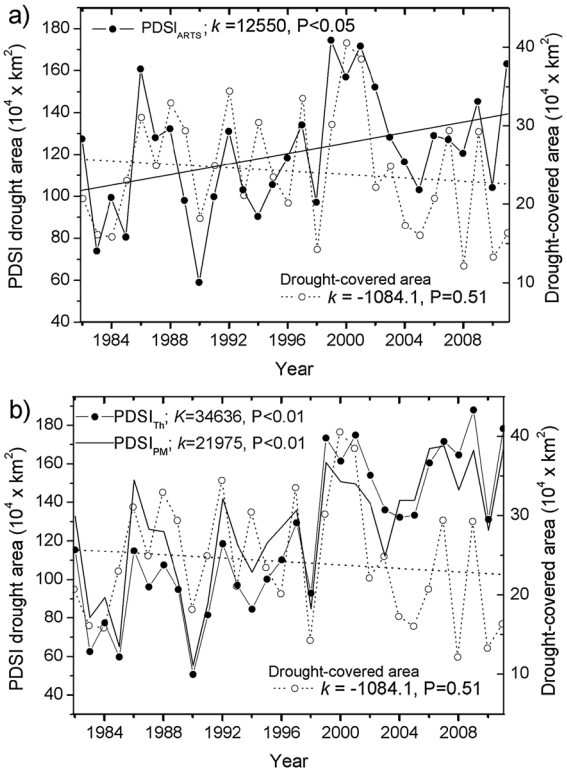

Figure 10. Time series of annual (a) drought-covered area from agriculture survey and $PDSI_{ARTS}$, (b) $PDSI_{Th}$ and $PDSI_{PM}$ drought area (defined as PDSI < -0.5) over cropland during 1982–2011 and their linear trends with slope k and significance P.

$PDSI_{ARTS}$ is more likely to simulate real drought condition and its impact on agriculture in China than $PDSI_{PM}$ and $PDSI_{Th}$.

As an independent data, drought-covered area from agriculture survey characterizes crop drought severity in China and provides a chance to evaluate drought indices. For instance, the drought-covered area data did not support the abrupt uptrend ($P < 0.01$) of drought area over China given by $PDSI_{Th}$ and $PDSI_{PM}$ (Figure 10b) and they had a poor relationship ($P > 0.2$). It should be cautious when PDSI model was applied to explaining climatic trend of crop drought area. The results of this study have implications for how we interpret agriculture drought trend derived from PDSI under global warming, atmosphere CO_2 increasing, and human impact.

6. Conclusions

A recently developed self-calibrating PDSI model, i.e., $PDSI_{ARTS}$ model, was applied to drought research in China during 1982–2011. Spatial-temporal changes of drought and its attributions were analyzed and compared with $PDSI_{Th}$ and $PDSI_{PM}$ as well as the drought area from agriculture survey in China.

Compared with the drying trend derived from $PDSI_{Th}$ and $PDSI_{PM}$, $PDSI_{ARTS}$ indicated nonsignificant change of drought in China under a warming climate for 1982–2011 because it accounts for more impacts of remote sensing vegetation LAI, sunshine duration, relative humility, wind speed besides air temperature, and precipitation on monthly scales. A warming climate did not necessarily result in a drying trend in China. As $PDSI_{ARTS}$ model was sensitive to the key driving variable of E_P, appropriate E_P such as ARTS E_0 rather than E_{P_Th} and E_{P_PM} should be adopted, otherwise a contrasting drying trend might result. Besides annual values of E_0 and P_r, their spatial patterns should be considered in evaluating drought condition for whole China because northern China dominated the drought variations of whole China while southern China played a minor role.

There existed different trend and spatial pattern of drought in China during 1990s and 2000s, respectively. China had a drying trend over 1990s featuring a spatial pattern of northern drought and southern wet, whereas a wetting trend was found in China during 2000s accompanied by a contrasting drought pattern of southern drought and northern wet. In addition, an extreme drought event occurred in 2000 and 2001, indicating a turning point, caused an unprecedented large area of agriculture drought during 1982–2011, which indicates a typical spatial pattern of severe drought in China on yearly scales, i.e., northern drought and southern wet.

Drought-covered area from agriculture survey was initially adopted to evaluate three PDSIs' performance in detecting agriculture drought area. We found that $PDSI_{ARTS}$-reflected nature drought still dominated interannual variations of drought area from agricultural survey. $PDSI_{ARTS}$ gave an increasing trend ($P < 0.05$) of agriculture drought area but more comparable to the survey than that ($P < 0.01$) of $PDSI_{Th}$ and $PDSI_{PM}$. In short, $PDSI_{ARTS}$ was more appropriate than $PDSI_{Th}$ and $PDSI_{PM}$ for detecting interannual variations of agricultural drought area in China. Due to regardless of impacts of atmosphere CO_2 increasing and cultivation technology on crop drought by current PDSI models, it should be cautious to deduce the climate trend of agriculture drought area from PDSI models.

Acknowledgments

We acknowledge the use of the global LAI3g data sets available at Department of Earth and Environment of Boston University (http://sites.bu.edu/cliveg/datacodes/), the agricultural drought-covered area data investigated by National Bureau of Statistics of China (http://data.stats.gov.cn/), climate data from National Meteorological Information Center (NMIC) of Chinese Meteorological Administration (http://cdc.nmic.cn/home.do), the Global Gridded Soil Data and ISLSCP II NOAA monthly albedo from Oak Ridge National Laboratory Distributed Active Archive Center (http://www.daac.ornl.gov). This work was supported by National Basic Research Program of China (2013CB430205), National Natural Science Foundation of China (41571327, 41171284), Chinese Academy of Sciences (XDA05050602-1), and partly funded by grants from a University of Virginia's Programs of Distinction grant to H.H. Shugart. The reviewers are thanked for their constructive remarks and suggestions.

References

Allen, L. H., Jr., V. G. Kakani, J. C. V. Vu, and K. J. Boote (2011), Elevated CO2 increases water use efficiency by sustaining photosynthesis of water-limited maize and sorghum, *J. Plant Physiol.*, *168*, 1909–1918, doi:10.1016/j.jplph.2011.05.005.

Allen, R. G. (1998), Crop evapotranspiration: Guidelines for computing crop water requirements. FAO irrigation and drainage paper No. 56, Food and Agriculture Organization of the United Nations.

Anderson, M. C., C. Hain, B. Wardlow, A. Pimstein, J. R. Mecikalski, and W. P. Kustas (2011), Evaluation of drought indices based on thermal remote sensing of evapotranspiration over the continental United States, *J. Clim.*, *24*, 2025–2044, doi:10.1175/2010jcli3812.1.

Anderson, M. C., C. Hain, J. Otkin, X. Zhan, K. Mo, M. Svoboda, B. Wardlow, and A. Pimstein (2013), An intercomparison of drought indicators based on thermal remote sensing and NLDAS-2 simulations with U.S. Drought Monitor classifications, *J. Hydrometeorol.*, *14*, 1035–1056, doi:10.1175/jhm-d-12-0140.1.

Brodribb, T. J., S. A. M. McAdam, G. J. Jordan, and T. S. Feild (2009), Evolution of stomatal responsiveness to CO2 and optimization of water-use efficiency among land plants, *New Phytol.*, *183*, 839–847, doi:10.1111/j.1469-8137.2009.02844.x.

Chen, J. M., P. D. Blanken, T. A. Black, M. Guilbeault, and S. Chen (1997), Radiation regime and canopy architecture in a boreal aspen forest, *Agric. Forest Meteorol.*, *86*, 107–125, doi:10.1016/S0168-1923(96)02402-1.

Csiszar, I. A. (2009), *ISLSCP II NOAA 5-Year Average Monthly Snow-Free Albedo From AVHRR*, Oak Ridge National Laboratory Distributed Active Archive Center, Oak Ridge, Tenn., doi:10.3334/ORNLDAAC/959.

Dai, A. (2011), Characteristics and trends in various forms of the Palmer Drought Severity Index during 1900–2008, *J. Geophys. Res.*, *116*, D12115, doi:10.1029/2010JD015541.

Global Soil Data Task Group (2000), *Global Gridded Surfaces of Selected Soil Characteristics (IGBP-DIS) Data Set*, Oak Ridge National Laboratory Distributed Active Archive Center, Oak Ridge, Tenn., doi:10.3334/ORNLDAAC/569.

Hartmann, D. L., et al. (2013), Observations: Atmosphere and surface. In: Climate change 2013: The physical science basis, in *Contribution of Working Group I to the Fifth Assessment Report of the Intergovernmental Panel on Climate Change*, edited by T. F. Stocker et al., Cambridge University Press, Cambridge, U. K., and New York.

Impens, I., and R. Lemeur (1969), Extinction of net radiation in different crop canopies, *Theor. Appl. Climatol.*, *17*, 403–412, doi:10.1007/bf02243377.

Karl, T. R. (1986), The sensitivity of the Palmer drought severity index and Palmer's Z-index to their calibration coefficients including potential evapotranspiration, *J. Climate Appl. Meteorol.*, *25*, 77–86, doi:10.1175/1520-0450(1986)025<0077:tsotpd>2.0.co;2.

Kelliher, F. M., R. Leuning, M. R. Raupach, and E. D. Schulze (1995), Maximum conductances for evaporation from global vegetation types, *Agric. Forest Meteorol.*, *73*, 1–16, doi:10.1016/0168-1923(94)02178-M.

Kogan, F. N. (1997), Global Drought Watch from Space, *Bull. Am. Meteorol. Soc.*, *78*, 621–636, doi:10.1175/1520-0477(1997)078<0621:gdwfs>2.0.co;2.

Lau, K. M., K. M. Kim, and S. Yang (2000), Dynamical and boundary forcing characteristics of regional components of the Asian summer monsoon, *J. Clim.*, *13*, 2461–2482, doi:10.1175/1520-0442(2000)013<2461:dabfco>2.0.co;2.

Li, D., H. Liu, Y. Qiao, Y. Wang, Z. Cai, B. Dong, C. Shi, Y. Liu, X. Li, and M. Liu (2013), Effects of elevated CO2 on the growth, seed yield, and water use efficiency of soybean (Glycine max (L.) Merr.) under drought stress, *Agric. Water Manag.*, *129*, 105–112, doi:10.1016/j.agwat.2013.07.014.

Li, J., E. Cook, R. D'arrigo, F. Chen, and X. Gou (2009), Moisture variability across China and Mongolia: 1951–2005, *Clim. Dyn.*, *32*, 1173–1186, doi:10.1007/s00382-008-0436-0.

Li, Y., R. Lu, and B. Dong (2007), The ENSO–Asian monsoon interaction in a coupled ocean–atmosphere GCM, *J. Clim.*, *20*, 5164–5177, doi:10.1175/jcli4289.1.

McKee, T. B., N. J. Doesken, and J. Kliest (1993), The relationship of drought frequency and duration to time scales, in *Proceedings of the 8th Conference of Applied Climatology*, pp. 179–184, Am. Meterol. Soc., Anaheim, Calif.

McNally, A., G. J. Husak, M. Brown, M. Carroll, C. Funk, S. Yatheendradas, K. Arsenault, C. Peters-Lidard, and J. P. Verdin (2015), Calculating crop water requirement satisfaction in the West Africa Sahel with remotely sensed soil moisture, *J. Hydrometeorol.*, *16*, 295–305, doi:10.1175/jhm-d-14-0049.1.

Mishra, A. K., and V. P. Singh (2010), A review of drought concepts, *J. Hydrol.*, *391*, 202–216, doi:10.1016/j.jhydrol.2010.07.012.

Mkhabela, M., P. Bullock, M. Gervais, G. Finlay, and H. Sapirstein (2010), Assessing indicators of agricultural drought impacts on spring wheat yield and quality on the Canadian prairies, *Agric. Forest Meteorol.*, *150*, 399–410, doi:10.1016/j.agrformet.2010.01.001.

Monteith, J. L. (1965), Evaporation and the environment, *Symp. Soc. Exp. Biol.*, *19*, 205–234.

Monteith, J. L., and M. H. Unsworth (1990), *Principles of Environmental Physics*, 2nd ed., Edward Arnold, London.

Mu, Q., M. Zhao, J. S. Kimball, N. G. McDowell, and S. W. Running (2013), A remotely sensed global terrestrial drought severity index, *Bull. Am. Meteorol. Soc.*, *94*, 83–98, doi:10.1175/bams-d-11-00213.1.

Narasimhan, B., and R. Srinivasan (2005), Development and evaluation of Soil Moisture Deficit Index (SMDI) and Evapotranspiration Deficit Index (ETDI) for agricultural drought monitoring, *Agric. Forest Meteorol.*, *133*, 69–88, doi:10.1016/j.agrformet.2005.07.012.

Owe, M., R. de Jeu, and T. Holmes (2008), Multisensor historical climatology of satellite-derived global land surface moisture, *J. Geophys. Res.*, *113*, F01002, doi:10.1029/2007JF000769.

Palmer, W. C. (1965), Meteorological drought, U.S. Weather Bureau Research Paper 45, pp 58.

Piao, S., et al. (2014), Evidence for a weakening relationship between interannual temperature variability and northern vegetation activity, *Nat. Commun.*, *5*, doi:10.1038/ncomms6018.

Poulter, B., et al. (2014), Contribution of semi-arid ecosystems to interannual variability of the global carbon cycle, *Nature*, *509*, 600–603, doi:10.1038/nature13376.

Priestley, C. H., and R. J. Taylor (1972), Assessment of surface heat-flux and evaporation using large-scale parameters, *Mon. Weather Rev.*, *100*, 81–92.

Shafer, B. A., and L. E. Dezman (1982), Development of a Surface Water Supply Index (SWSI) to assess the severity of drought conditions in snowpack runoff areas, in *Proceedings of the 50th Annual Western Snow Conference*, pp. 164–75, Colo. State Univ., Fort Collins.

Sheffield, J., and E. Wood (2008), Projected changes in drought occurrence under future global warming from multi-model, multi-scenario, IPCC AR4 simulations, *Clim. Dyn.*, *31*, 79–105, doi:10.1007/s00382-007-0340-z.

Sheffield, J., E. F. Wood, and M. L. Roderick (2012), Little change in global drought over the past 60 years, *Nature*, *491*, 435–438, doi:10.1038/nature11575.

Shen, C., W.-C. Wang, Z. Hao, and W. Gong (2007), Exceptional drought events over eastern China during the last five centuries, *Clim. Change*, *85*, 453–471, doi:10.1007/s10584-007-9283-y.

Sun, Y., and Y. Ding (2010), A projection of future changes in summer precipitation and monsoon in East Asia, *Sci. China Earth Sci.*, *53*, 284–300, doi:10.1007/s11430-009-0123-y.

Thornthwaite, C. W. (1948), An approach toward a rational classification of climate, *Geogr. Rev.*, *38*, 55–94.

Trenberth, K. E., A. Dai, G. van der Schrier, P. D. Jones, J. Barichivich, K. R. Briffa, and J. Sheffield (2014), Global warming and changes in drought, *Nat. Clim. Change*, *4*, 17–22, doi:10.1038/nclimate2067.

Tsakiris, G., and H. Vangelis (2005), Establishing a drought index incorporating evapotranspiration, *Eur. Water*, *9/10*, 3–11.

Tuba, Z., K. Szente, and J. Koch (1994), Response of photosynthesis, stomatal conductance, water use efficiency and production to long-term elevated CO2 in winter wheat, *J. Plant Physiol.*, *144*, 661–668, doi:10.1016/S0176-1617(11)80657-7.

van der Schrier, G., P. D. Jones, and K. R. Briffa (2011), The sensitivity of the PDSI to the Thornthwaite and Penman-Monteith parameterizations for potential evapotranspiration, *J. Geophys. Res.*, *116*, D03106, doi:10.1029/2010JD015001.

Vicente-Serrano, S. M., S. Beguería, J. Lorenzo-Lacruz, J. J. Camarero, J. I. López-Moreno, C. Azorin-Molina, J. Revuelto, E. Morán-Tejeda, and A. Sanchez-Lorenzo (2012), Performance of drought indices for ecological, agricultural, and hydrological applications, *Earth Interact.*, *16*, 1–27, doi:10.1175/2012ei000434.1.

Vu, J. C. V., and L. H. Allen Jr. (2009), Growth at elevated CO2 delays the adverse effects of drought stress on leaf photosynthesis of the C4 sugarcane, *J. Plant Physiol.*, *166*, 107–116, doi:10.1016/j.jplph.2008.02.009.

Wang, A., D. P. Lettenmaier, and J. Sheffield (2011), Soil moisture drought in China, 1950–2006, *J. Clim.*, *24*, 3257–3271, doi:10.1175/2011jcli3733.1.

Wang, Q., P. Shi, T. Lei, G. Geng, J. Liu, X. Mo, X. Li, H. Zhou, and J. Wu (2015), The alleviating trend of drought in the Huang-Huai-Hai Plain of China based on the daily SPEI, *Int. J. Climatol.*, doi:10.1002/joc.4244.

Wang, S., et al. (2015), Improving the light use efficiency model for simulating terrestrial vegetation gross primary production by the inclusion of diffuse radiation across ecosystems in China, *Ecol. Complex.*, *23*, 1–13, doi:10.1016/j.ecocom.2015.04.004.

Wells, N., S. Goddard, and M. J. Hayes (2004), A self-calibrating Palmer drought severity index, *J. Clim.*, *17*, 2335–2351, doi:10.1175/1520-0442(2004)017<2335:ASPDSI>2.0.CO;2.

Wu, P., J. Jin, and X. Zhao (2010), Impact of climate change and irrigation technology advancement on agricultural water use in China, *Clim. Change*, *100*, 797–805, doi:10.1007/s10584-010-9860-3.

Xu, K., D. Yang, H. Yang, Z. Li, Y. Qin, and Y. Shen (2014), Spatio-temporal variation of drought in China during 1961–2012: A climatic perspective, *J. Hydrol.*, doi:10.1016/j.jhydrol.2014.09.047.

Yan, H., and H. H. Shugart (2010), An air relative-humidity-based evapotranspiration model from eddy covariance data, *J. Geophys. Res.*, *115*, D16106, doi:10.1029/2009JD013598.

Yan, H., et al. (2012), Global estimation of evapotranspiration using a leaf area index-based surface energy and water balance model, *Remote Sens. Environ.*, *124*, 581–595, doi:10.1016/j.rse.2012.06.004.

Yan, H., Q. Yu, Z.-C. Zhu, R. B. Myneni, H.-M. Yan, S.-Q. Wang, and H. H. Shugart (2013), Diagnostic analysis of interannual variation of global land evapotranspiration over 1982–2011: Assessing the impact of ENSO, *J. Geophys. Res. Atmos.*, *118*, 8969–8983, doi:10.1002/jgrd.50693.

Yan, H., S.-Q. Wang, H.-Q. Lu, Q. Yu, Z.-C. Zhu, R. B. Myneni, Q. Liu, and H. H. Shugart (2014), Development of a remotely sensing seasonal vegetation-based Palmer Drought Severity Index and its application of global drought monitoring over 1982–2011, *J. Geophys. Res. Atmos.*, *119*, 9419–9440, doi:10.1002/2014JD021673.

Yu, C., et al. (2014b), Dynamic assessment of the impact of drought on agricultural yield and scale-dependent return periods over large geographic regions, *Environ. Modell. Software*, *62*, 454–464, doi:10.1016/j.envsoft.2014.08.004.

Yu, M., Q. Li, M. J. Hayes, M. D. Svoboda, and R. R. Heim (2014a), Are droughts becoming more frequent or severe in China based on the Standardized Precipitation Evapotranspiration Index: 1951–2010?, *Int. J. Climatol.*, *34*, 545–558, doi:10.1002/joc.3701.

Zhai, J. Q., B. D. Su, V. Krysanova, T. Vetter, C. Gao, and T. Jiang (2010), Spatial variation and trends in PDSI and SPI indices and their relation to streamflow in 10 large regions of China, *J. Clim.*, *23*, 649–663, doi:10.1175/2009JCLI2968.1.

Zhang, L., and T. Zhou (2015), Drought over East Asia: A review, *J. Clim.*, *28*, 3375–3399, doi:10.1175/jcli-d-14-00259.1.

Zhang, L., B. F. Wu, X. S. Li, and Q. Xing (2014), Classification system of China land cover for carbon budget [in Chinese], *Acta Ecol. Sin.*, *34*, 7158–7166, doi:10.5846/stxb201310102431.

Zhou, T.-J., and R.-C. Yu (2005), Atmospheric water vapor transport associated with typical anomalous summer rainfall patterns in China, *J. Geophys. Res.*, *110*, D08104, doi:10.1029/2004JD005413.

Zhu, Z., J. Bi, Y. Pan, S. Ganguly, A. Anav, L. Xu, A. Samanta, S. Piao, R. Nemani, and R. Myneni (2013), Global data sets of vegetation leaf area index (LAI)3 g and fraction of photosynthetically active radiation (FPAR)3 g derived from Global Inventory Modeling and Mapping Studies (GIMMS) normalized difference vegetation index (NDVI3g) for the period 1981 to 2011, *Remote Sens.*, *5*, 927–948, doi:10.3390/rs5020927.

Zou, X., P. Zhai, and Q. Zhang (2005), Variations in droughts over China: 1951–2003, *Geophys. Res. Lett.*, *32*, L04707, doi:10.1029/2004GL021853.